Selective Activation of GPCRs: Molecular Dynamics Shows Siponimod Binds but Fails to Activate S1PR2 Unlike S1PR1

Kumari Soniya,[1] Chanukya Nanduru,[1] and Antarip Halder[1]
[1]*Aganitha.ai, 512T, Road number 29, Jubilee Hills, Hyderabad, Telangana-500033, India*

(*Electronic mail: antarip@aganitha.ai)

(Dated: 30 September 2024)

Understanding drug selectivity is crucial for designing effective medications that target specific proteins while minimizing off-target interactions, thus optimizing therapeutic outcomes. Biochemical and cellular assays provide functional insights but often lack detailed molecular understanding of selectivity in large families of similar proteins. In such cases, computational studies can complement experimental approaches to fill gaps in understanding drug selectivity. In this study, Molecular Dynamics (MD) simulation methods have been used to examine the selective modulation of sphingosine-1-phosphate receptor 1 (S1PR1) over S1PR2 by Siponimod, an FDA-approved drug for Multiple Sclerosis. Both S1PR1 and S1PR2 belong to the same sub-family of G Protein-Coupled Receptors (GPCRs). Contrary to the previous hypothesis based on molecular docking, MD simulations showed that Siponimod can bind to S1PR2 with an *in silico*-determined affinity comparable to that of S1PR1. Comparing the dynamics of Siponimod-bound S1PR2 with S1P-bound S1PR2 revealed that the transmission switches necessary for downstream biological activity are activated by S1P but not by Siponimod, whereas both S1P and Siponimod activate those transmission switches in S1PR1. A few crucial residues in S1PR2 were also identified that can be leveraged to optimize molecules to bind selectively to S1PR1 over S1PR2. Through our study, we showed that *in silico* approaches can help in understanding the ligand-induced structural changes and aid in developing and optimizing drugs for GPCRs, the most abundant class of membrane proteins in the human genome and the largest family of membrane receptors targeted by approved drugs.

I. INTRODUCTION

G protein-coupled receptors (GPCRs) constitute the most prevalent class of integral membrane proteins encoded in the human genome[1]. Additionally, they comprise the largest family of membrane receptors that are the focus of approved pharmaceutical interventions[2]. However, designing a drug targeting GPCRs is challenging due to the high sequence and structural homology among members of the same sub-family, making it difficult to achieve selectivity. This similarity increases the risk of off-target effects, necessitating precise molecular design to differentiate between closely related receptors[3,4].

Among ∼800 GPCRs encoded in the human genome, five of the class A GPCRs are found to be highly specific towards sphingosine-1-phosphate (S1P) binding[5]. These are known as S1P receptors (S1PR1 through S1PR5). S1P, a signaling lysophospholipid, is produced by the phosphorylation of sphingosine via either sphingosine kinase 1 or sphingosine kinase 2[6]. The S1P gradient regulates immune cell traffic between lymphoid organs and circulation through S1PR1[7]. When S1PR1 binds to S1P, it undergoes internalization, reducing receptor presence on the cell surface and preventing lymphocytes from sensing the S1P gradient. As a result, lymphocytes are confined within lymphoid tissues[8,9]. This mechanism makes S1PR1 a valuable target for treating autoimmune diseases such as Multiple Sclerosis (MS)[10–12], tackling transplant rejections, and addressing conditions like Pulmonary Fibrosis[11,13,14]. The receptor subtypes S1PR1, S1PR2 and S1PR3 are primarily expressed in the cardiovascular, central nervous, and immune systems, whereas the expression of S1PR4 and S1PR5 is restricted to the immune and nervous systems[15,16]. S1PR2 is also linked with deafness in mice if the gene is mutated or knocked out.[17,18]

Certainly, while designing drugs for S1PR1, it is ideal to ensure that the drugs do not modulate other receptors, specifically S1PR2 and S1PR3 due to their involvement with cardiac system. For example, the first-in-class approved drug for MS, Fingolimod (FTY720), is known to be active against all S1P receptors except S1PR2[3,19]. Activation of S1PR3 by Fingolimod is associated with heart conditions such as bradycardia.[20,21] Hence, this limits the clinical use of Fingolimod. In contrast, second-generation S1P receptor modulators such as Siponimod, Ozanimod, and Ponesimod are more selective for S1PR1 and S1PR5 over S1PR2, S1PR3, and S1PR4, resulting in fewer side effects[9,11,12]. Understanding the mechanisms of action of these next-generation drugs is crucial for developing strategies to enhance drug selectivity in GPCR therapeutics.

Functional assays, such as the GTPγ[^{35}S]-binding assay, are commonly employed to assess the activity of ligands against GPCRs[22,23]. When agonists bind to GPCRs, they induce conformational changes in the receptor, leading to the dissociation of the α subunit from the β and γ subunits of the heterotrimeric G protein complex[24]. This assay measures the radioactivity of GTPγ[^{35}S] that binds to the Gα subunit by displacing GDP from the binding pocket. However, these assays cannot differentiate whether G-protein activation failed due to the ligand not binding to the active site or failing to induce the necessary structural changes despite binding. Siponimod is a second-generation approved treatment in adults for the relapsing forms of Multiple Sclerosis (MS) that includes the clinically isolated syndrome, relapsing- remitting MS, and active secondary progressive MS[25,26]. *In vitro* studies using GTPγ[^{35}S]-binding assay reported that the half maximal effective concentrations (EC50) for Siponimod in human S1PR1 and S1PR5 are ≈0.46 nM and ≈ 0.3 nM, respectively. In contrast, the EC50 for S1PR2, S1PR3 and S1PR4 are >

10,000 nM, > 1111 nM and ≈383.7 nM, respectively[22,27]. So, it is evident that Siponimod selectively modulates S1PR1 and S1PR5 over S1PR2, S1PR3, and S1PR4. Also, radioligand binding assays confirm Siponimod's binding at the active site (i.e., the S1P binding site) of human S1PR1 and S1PR5 but the results for the same are not available for the other three receptors that Siponimod fails to modulate[27]. Therefore, the precise mechanism behind Siponimod's selectivity remains unclear, highlighting the need for further investigation to understand its mode of action and improve drug design strategies in GPCR therapeutics.

Meticulously designed computational studies have the potential to complement experimental methods and help overcome their limitations, particularly in the context of drug design[28]. In this study, we utilized a range of bioinformatics and computational chemistry techniques to explore the potential binding of Siponimod to the active site of S1PR1 and S1PR2. Previous computational approaches suggested that Siponimod's lower selectivity for S1PR2 might be due to steric clashes with a phenylalanine residue (F274) upon docking to its active site[29]. However, this hypothesis was based on an engineered active site of S1PR2 derived from a cryo-EM structure of Siponimod-bound S1PR1. Recently, the cryo-EM structure of S1P-bound S1PR2 has been resolved[17], providing an opportunity to investigate Siponimod's binding potential to S1PR2 using more accurate computational methods. Our analyses, involving structure modeling, molecular docking, and microsecond timescale atomistic Molecular Dynamics (MD) simulations, indicate that Siponimod can bind to the active site of S1PR2. Despite this strong binding, our results show that Siponimod fails to induce the necessary conformational changes in the activation switches of S1PR2. We propose that Siponimod's inability to activate S1PR2 is due to its lack of interaction with certain key active site residues, which it interacts with in S1PR1. Targeting these residues in future drug design efforts could enhance selectivity.

II. METHODS AND TOOLS

Sequence alignment of S1PR1 and S1PR2 was performed using NCBI BLASTp[30,31] server to determine the percentage sequence similarity between the two S1P receptors.

Structure modelling of S1PR1 and S1PR2: The general architecture of the seven transmembrane helices along with extracellular and intracellular loops in S1PRs are illustrated in Figure 1a. Important transmission switches, ERY(H) and NPxxY motifs along with most conserved residues as per Ballesteros Weinstein (BW)[32] numbering schemes are depicted in the snake plot[33,34]. For *in silico* investigations, we selected the latest cryo-EM structures of human S1PR1 (PDB ID: 7TD3[29]) and S1PR2 (PDB ID: 7T6B[17]) that are complexed with the native ligand S1P and with the G proteins in the cytoplasmic regions. This will ensure that the S1P receptors are in their respective active state conformations. For the next steps we focused only on the S1PR chains, i.e. chain D in 7TD3 and chain E in 7T6B. Missing residues in both the chains, except the highly disordered N and C terminal residues, were modelled using Swiss modeler server[35]. The final modeled S1PR1 and S1PR2 chains have 304 and 279 residues, respectively. The first 21 residues in the N-terminal are missing in final modelled S1PR1 and the first 11 N-terminal residues are missing in the final modelled S1PR2. The residue numbering was adjusted accordingly. The structural similarity between the final modeled structures of S1PR1 and S1PR2 was assessed using Foldseek[36]. Foldseek performs structural alignment by utilizing a structural alphabet that emphasizes tertiary interactions rather than the protein backbone. This method generates a TM-score[37] to quantify structural similarity, ranging from 0 to 1. A higher TM-score indicates greater structural similarity between the two proteins.

Molecular docking: Molecular docking was performed using AutoDock VINA[38,39] utility in UCSF Chimera[40] with default settings. S1P and Siponimod were docked at the S1P binding site (illustrated in Figure 1c) of both S1PR1 and S1PR2. Different non-covalent interactions forming between the docked ligand and the binding site residues were analyzed using Protein-Ligand Interaction Profiler (PLIP)[41]. The docked poses with the highest docking scores were used for building the initial structures for performing MD simulations. To mimic the cellular environment in the MD simulations, ligand free and ligand bound receptors were embedded in lipid environment and surrounded by water as illustrated in Figure 1b. All-atom unbiased MD simulations were performed on six systems, viz., (i) Siponimod bound S1PR1 (Siponimod-S1PR1), (ii) Siponimod bound S1PR2 (Siponimod-S1PR2), (iii) S1P bound S1PR1 (S1P-S1PR1), (iv) S1P bound S1PR2 (S1P-S1PR2), (v) ligand free S1PR1 (apo S1PR1) and (vi) ligand free S1PR2 (apo S1PR2).

Setting up MD simulations: The MD systems were prepared using a set of utilities present in AmberTools22[42]. Force fields for S1P and Siponimod were generated with AM1-BCC charges[43,44] in antechamber[45,46]. Protein was embedded in the POPC (1-palmitoyl-2- oleoyl-sn-glycero-3-phosphocholine) layer with proper alignment using PACKMOL-Memgen[47] tool in AmberTools22. Lipid21 force field[48] was used for the lipid bilayer. The systems were hydrated with a three-point SPC/E[49,50] water model in a cubic box with 8 Å buffer. Chloride ions were added to neutralize the system. The system was then minimized using sander engine on single CPU. Minimization was carried out using steepest descent algorithm for the first 25,000 cycles, and conjugate gradient algorithm was used for last 25,000 cycles. AMBER minimized topology and coordinate files of the systems were converted to GROMACS compatible format using ParmEd python utility. Minimization, NVT equilibration followed by NPT equilibration and NPT production run were carried out in GPU enabled GROMACS 2022.3[51–53] following well-established protocols as discussed in detail in the SI. For each of the six systems 1 μs long MD trajectory was generated for further analysis. For the four ligand bound cases (i-iv), a second replica of 1 μs was run for statistical validation of the observed conformational differences.

Analysing MD trajectories: The MD trajectories were visualized using Visual Molecular Dynamics (VMD 1.9.4) tool[54] and analyzed using GROMACS and AmberTools22.

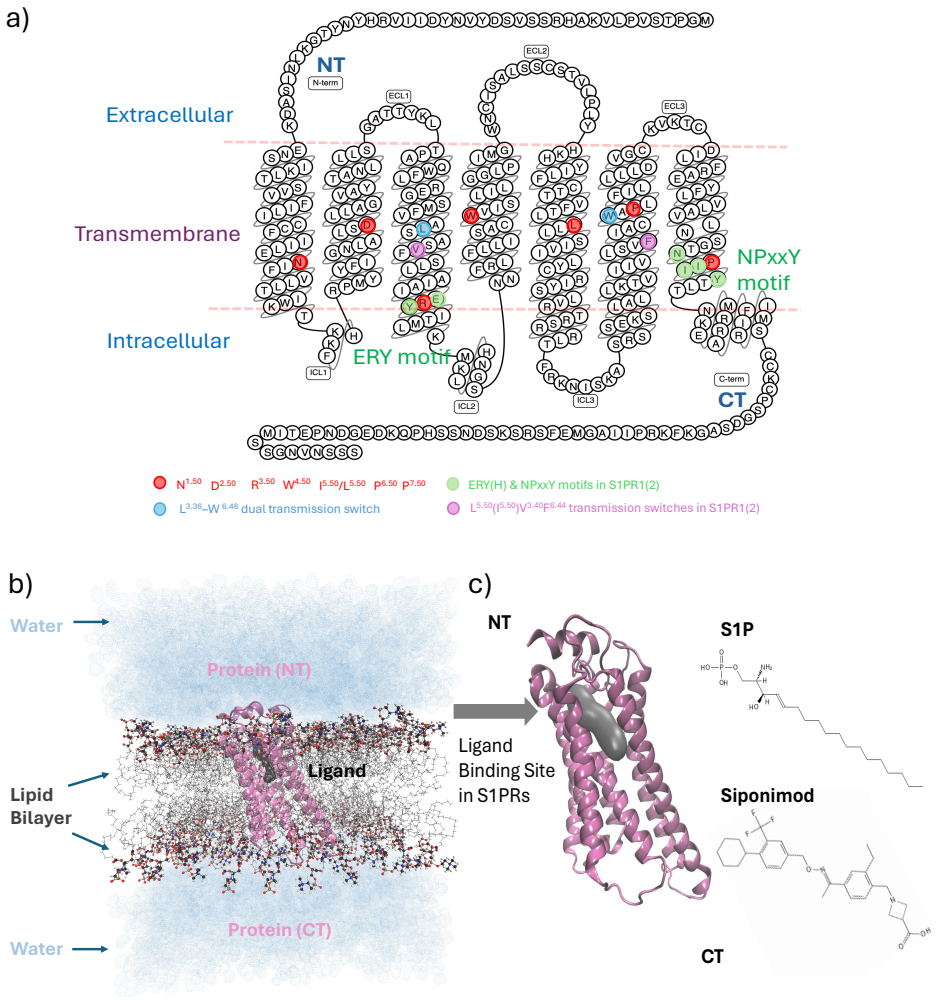

FIG. 1. System details for S1P receptors. a) Snake plot (using S1PR1 as reference) depicting the most conserved residues of the Transmembrane (TM) helices in S1PRs (red), important toggle switches (blue) and conserved ERY(H) and NPxxY motifs (green) in S1PRs; b) MD simulation system consisting of ligand bound S1P receptors inside lipid bilayer in aqueous medium; c) S1P and Siponimod binds towards the N-terminal (NT) end of the receptors occupying same binding pocket as shown in blue surface.

Fluctuations in receptors during the simulation trajectories were measured by Root Mean Square Displacement (RMSD) with respect to the initial structure and Root Mean Square Fluctuations (RMSF) averaged over the entire trajectory. For quantifying the relative dynamics of different parts of the receptors, Dynamic Cross- Correlation Maps (DCCM) and Principal Component Analysis (PCA)[55] were obtained using CPPTRAJ utility[56] from AmberTools22.

Relative binding free energies of the ligand-bound receptors were obtained from MMGBSA calculations[57] performed using the gmx_MMPBSA package[58]. A single trajectory approach using modified Gibbs-Boltzmann protocol was followed[59]. To elucidate the chemistry of ligand-protein interactions, we analyzed the residue-wise contribution towards ligand binding free energies. The step-wise protocol followed to consolidate the data from two independent replicas is discussed in the SI.

III. RESULTS AND DISCUSSION

This study explores the selective modulation of S1PR1 over S1PR2 by Siponimod using a comprehensive array of *in silico* methods, including protein sequence and structure alignment, molecular docking, and all-atom conventional MD simulations. The BW numbering scheme is utilized in this article to identify the residues in the transmembrane helices.

A. Active sites of both S1PR1 and S1PR2 have high structural similarity

The sequence and structural similarities between the two S1P receptors, S1PR1 and S1PR2, were analyzed in detail. A sequence alignment using the NCBI BLASTp server reveals that these two sequences share only about 50% similarity (Figure SI 1). Despite this modest sequence similarity, the

proteins exhibit high structural similarity, as evidenced by a TM-score of 0.88 obtained from Foldseek (Figure SI 2). This is expected since both receptors are members of the S1P receptor sub-family. The transmembrane helices and the overall fold, particularly the configuration of the S1P binding pocket (the active site), are nearly identical in both receptors. Minor structural differences are primarily due to variations in the orientations of the extracellular (ECL) and intracellular (ICL) loops (Figure SI 2). Given the structural similarities of the active sites in S1PR1 and S1PR2 and considering that Siponimod binds to the active site of S1PR1, it is reasonable to hypothesize that Siponimod will also bind to the active site of S1PR2.

While most residues involved in ligand binding and activation mechanisms are conserved, the sequence alignment indicates a few notable differences (Figure SI 1). For example, leucine ($L^{7.39}$) in S1PR1 is replaced by phenylalanine ($F274/F^{7.39}$) in S1PR2, highlighted in pink in Figure SI 1. Other similar differences are discussed in the SI. Although both leucine and phenylalanine have hydrophobic side chains, phenylalanine's bulkier phenyl group was previously hypothesized[29] to cause a steric clash, preventing Siponimod from binding to the active site of S1PR2 based on studies using an engineered binding pocket. However, with the availability of the S1P-bound S1PR2 structure[17], we can now re-evaluate this hypothesis and determine whether Siponimod can indeed bind to the active site of S1PR2.

B. Molecular docking suggests Siponimod can bind strongly to the active sites of both S1PR1 and S1PR2

We utilized molecular docking to compare the binding affinities of both S1P and Siponimod to the active sites of S1PR1 and S1PR2. At the outset of the discussion, it is important to note that experimentally determined structures of S1P-bound S1PR1 and S1PR2 were used in this study. The apo and Siponimod-bound systems for S1PR1 and S1PR2 were prepared from these S1P-bound protein structures, suggesting that the initial structures of S1PR1 and S1PR2 were already in an active conformation. Siponimod was then docked to the active conformations of both receptors. Both S1P and Siponimod occupy the same space inside the active site with polar head facing the extracellular region and the non-polar tails buried in the hydrophobic pocket near the transmission switches. A recent study[27] reveals that the molecular docking analysis of diverse S1PR modulators to the active sites of both S1PR1 and S1PR5 exhibited a good correlation with experimental data.

The binding affinity of Siponimod for S1PR2 (-13 kcal/mol) was ≈1.5 kcal/mol higher than that for S1PR1 (-11.7 kcal/mol). Additionally, contrary to the previous hypothesis[29], the docked pose of Siponimod showed no steric clashes with $F^{7.39}$ (F274) at the S1PR2 binding site (Figure 2c). These findings indicate that Siponimod not only binds to both receptors but also exhibits a slightly stronger binding affinity for S1PR2. A comparison of the ligand-protein interaction patterns of Siponimod with S1PR1 and S1PR2 shows that most of Siponimod's interactions with both the receptors are through π-stacking and hydrophobic interactions, with additional salt bridge interactions with ARG^{ECL1} in S1PR2. This explains its higher binding affinity compared to S1PR1 (Figure 2a & Figure 2c). Of particular importance is Siponimod's hydrogen bond interaction with $ASN^{2.60}$ in both S1PR1 and S1PR2.

S1P engages the N-terminal residues by forming hydrogen bonds and salt bridges with its phosphate head group, and the hydrophobic residues of the receptors interact with the lipid-like tail of S1P (Figure 2b & Figure 2d). In S1PR2, a salt bridge between ARG^{NT} and the phosphate head of S1P is also observed.

To validate the docking protocol, the docked conformation of Siponimod in S1PR1 was compared with its conformation in the cryo-EM structure of Siponimod-bound S1PR1 (PDB ID 7TD4). Typically, an RMSD of less than 2 Å between the docked pose and the reference structure (i.e., ligand pose from the crystal structure) is considered sufficiently accurate for ligand docking[60,61]. For Siponimod, the hydrophobic tail of the docked pose aligned well with the crystal structure pose, though there was a noticeable shift in the hydrophilic head, resulting in an RMSD (symmetry corrected) of approximately 1.8 Å between the two poses (Figure SI 3), which is acceptable. Since the same docking protocol was used to obtain the Siponimod bound S1PR2 structure, its reliability is supported. However, a comparison of the interactions of docked Siponimod in S1PR1 with experimentally determined Siponimod bound S1PR1 interactions revealed that, due to a different orientation of the polar head group at the N-terminal in the docked structure, interactions with LYS^{NT}, ARG^{ECL1}, and GLY^{ECL1} were absent in the docked pose of Siponimod in S1PR1 (Figure 2e).

The degrees of freedom of the protein residues were not considered during the rigid docking process, resulting in a static depiction of protein-ligand interactions. To understand these interactions more precisely, it is essential to consider the dynamics of the protein upon ligand binding. Therefore, all-atom unbiased MD simulations of both ligand-free and ligand-bound (S1P & Siponimod) S1PR1 and S1PR2 proteins embedded within lipid bilayers were conducted. This approach enables the comparison of (a) the binding free energy of the ligands, (b) the persistence of various protein-ligand interactions, (c) the impact of ligand binding on the structural dynamics of protein residues, and (d) the coordinated motions of the transmembrane helices.

C. MD simulations confirm Siponimod's binding to the active site of S1PR2

The MD trajectories were examined for the extent of fluctuations. As expected, residues corresponding to the loop regions have higher freedom to move thus showing higher RMSF values in both S1PR1 and S1PR2 systems. This holds true for both the replicas of the ≈1μs trajectories.(Figure SI 4a-4d). In the case of S1PR1, in the first replica, the RMSD fluctuations stabilized after ≈200 ns in apo and S1P bound

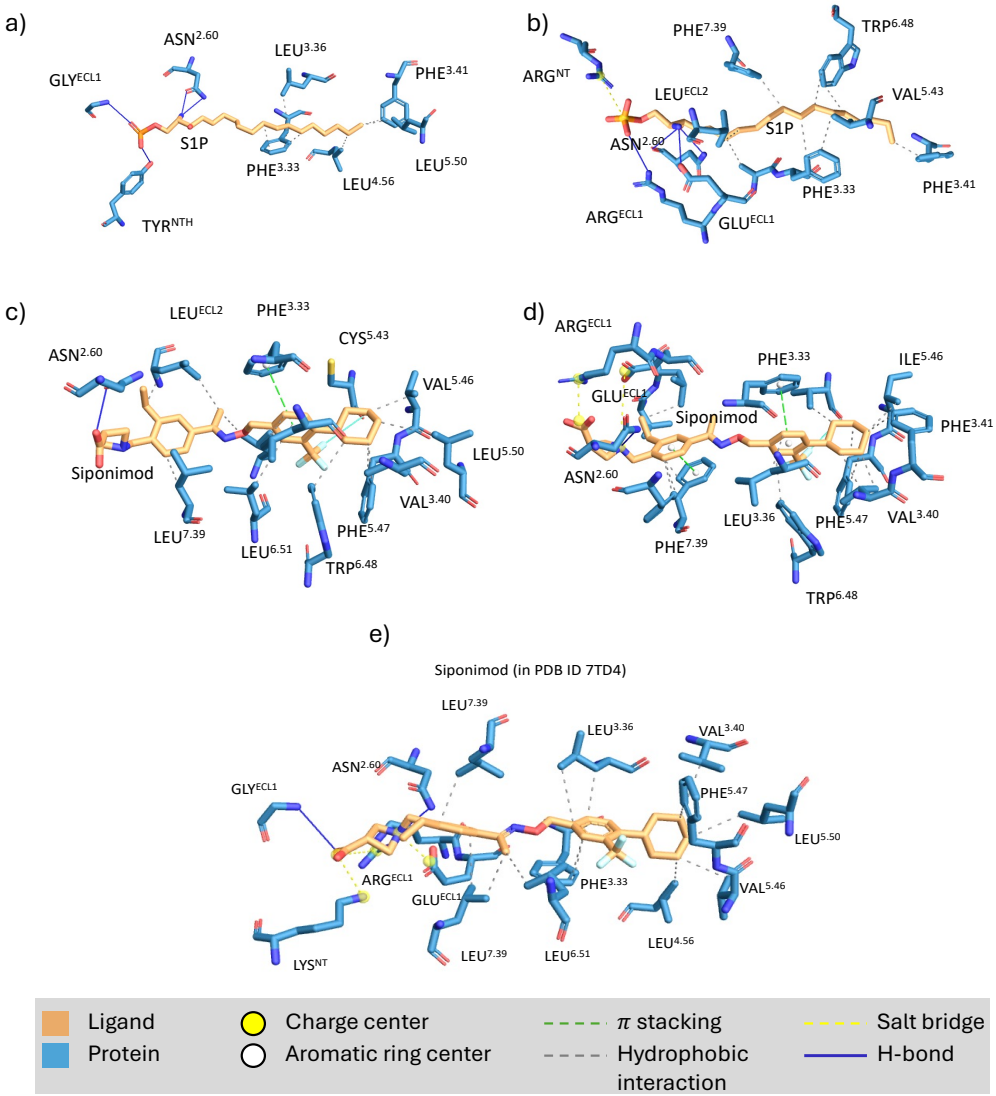

FIG. 2. PLIP analysis on the ligand bound S1PR1 and S1PR2 conformations obtained from docking: Hydrophilic head in S1P and Siponimod is engaged in hydrogen bonding with extracellular residues and the aliphatic chain is involved in hydrophobic interactions a) S1P bound S1PR1; b) S1P bound S1PR2; c) Siponimod bound S1PR1; d) Siponimod bound S1PR2; e) Siponimod bound S1PR1 in experimental structure.

receptor and after ≈500 ns for the Siponimod bound receptor (Figure SI 5a & SI 5b). RMSD fluctuations for all the three systems related to S1PR2 stabilized after ≈300 ns (Figure SI 5a & SI 5b). In the second replica, all the ligand bound systems reach stability after ≈100 ns (Figure SI 5c & SI 5d). The distribution of the first two principal components, calculated from the entire ≈2μs trajectory combining both replicas, indicates that the two replicas explore distinct, non-overlapping regions of the conformational space (Figure SI 6).

To maintain uniformity, MMGBSA calculations, along with pair-wise residue decomposition analysis, were performed on the last 500 ns (of the total 1 μs) trajectory, during which stable RMSD fluctuations were observed in all six cases in both the replicas. The relative binding free energies obtained from MMGBSA method ($\Delta G^{binding}_{MMGBSA}$) were also obtained for 5 short 20 ns replicas and are in good agreement with the values obtained from the longer trajectories (Table 1). Siponimod binds strongly at the active sites of both the receptors S1PR1 and S1PR2, as also suggested by the docking studies. However, the docking studies were unable to capture that the binding strength of Siponimod towards S1PR1 and S1PR2 are comparable. In both the cases, the $\Delta G^{binding}_{MMGBSA}$ values vary between -60 to -70 kcal/mol.

As per the $\Delta G^{binding}_{MMGBSA}$ values, the native ligand S1P binds to both receptors with a stronger affinity compared to the approved drug Siponimod (Table 1). Again, binding strength of S1P towards S1PR1 ($\Delta G^{binding}_{MMGBSA} \approx$ -74.7 to -94.9 kcal/mol) is higher than that towards S1PR2 ($\Delta G^{binding}_{MMGBSA} \approx$ -68.5 to -82.7 kcal/mol).

Our results also align well with the experimentally re-

TABLE I. Comparison of the ligand binding free energies ($\Delta G^{binding}_{MMGBSA}$) obtained from MMGBSA calculations performed on different replica of independent MD simulations: entire trajectories of five shorter (≈20 ns) replicas and the last 500 ns trajectories of the two longer (≈1 μs) replicas. The $\Delta G^{binding}_{MMGBSA}$ are reported in kcal/mol. The experimentally determined pEC50 values are obtained from the PHAROS database.

$\Delta G^{binding}_{MMGBSA}$ of	20 ns long replicas					1 μs long replicas		Experimental (pEC50)	Docking score (kcal/mol)
	1	2	3	4	5	1	2		
S1P to S1PR1	-94.5 ±7.6	-94.9 ±8.6	-94.7 ±6.1	-91.57 ±4.8	-92.7 ±7.2	-77.8 ±5.0	-74.7 ±6.4	10.57	-5.8
Siponimod to S1PR1	-61.8 ±2.7	-60.9 ±2.5	-61.9 ±3.0	-66.8 ±3.1	-65.9 ±3.4	-60.6 ±1.0	-63.4 ±3.4	9.41	-11.7
S1P to S1PR2	-74.1 ±4.4	-70.7 ±5.8	-69.9 ±4.4	-72.7 ±4.6	-68.5 ±4.2	-68.5 ±5.0	-82.7 ±7.0	9.64	-7.7
Siponimod to S1PR2	-67.8 ±2.5	-65.9 ±2.9	-68.7 ±2.6	-68.2 ±3.3	-67.1 ±3.0	-67.8 ±2.0	-60.7 ±2.9	NA*	-13.0

ported activity values, except for Siponimod-S1PR2 system. The pEC50 values for S1P and Siponimod against S1PR1 are 10.57 and 9.41, respectively (source: PHAROS database[62–64]). This indicates a higher affinity of S1P for S1PR1 compared to Siponimod. Additionally, the affinity of S1P for S1PR2 (pEC50 = 9.64) is reported to be[22,27] lower than its affinity for S1PR1. However, for Siponimod-S1PR2, the EC50 value is reported to be > 10000 nM. As previously mentioned, these values are derived from the GTPγ[^{35}S] functional assay, which does not necessarily evaluate whether Siponimod can bind to S1PR2, but only evaluates the activation of S1PR2 by Siponimod. Note that, evidence of S1P and Siponimod binding to the same active site in S1PR1 has been reported using competitive radioligand binding assays[22,27]. Cryo-EM structure of S1P-bound S1PR2 has also been solved[17]. But, to our knowledge, there is no reported study on Siponimod binding to S1PR2 using competitive radioligand binding assays or equivalent experimental methods. Hence, the experimental reports remain ambiguous regarding Siponimod's binding to S1PR2.

Computational studies performed in this work suggest that Siponimod can bind to the active site of S1PR2, while experimental reports indicate that Siponimod cannot modulate S1PR2 activity. To reconcile these findings, we aim to investigate whether Siponimod indeed binds to the active site of S1PR2 but fails to induce the structural changes necessary for modulation. The following sections will delve into these investigations, exploring the underlying mechanisms and potential implications.

D. Siponimod utilizes different binding strategies at the active sites of S1PR1 and S1PR2

Siponimod and S1P utilize a similar general strategy for binding to the active site of S1PR1. In both cases, the polar head region engages in electrostatic interactions with active site residues, while the nonpolar tail is stabilized by hydrophobic interactions. The phosphate group on the S1P ligand forms salt bridges and strong hydrogen bonds with the N-terminal region of the receptor. Similarly, Siponimod's polar head is stabilized within the pocket through hydrogen bonding interactions. However, a more detailed investigation reveals notable differences between the two ligands' binding modes.

Pairwise energy decomposition analysis (Figure 3a & 3b) reveals that in S1PR1, there are 15 common residues that significantly contribute to stabilizing both S1P and Siponimod binding at the active site. Additionally, four specific residues (SER105, TYR29, ASN101, and ARG120) interact strongly with S1P but do not engage with Siponimod. Conversely, three residues (MET124, ALA293, and GLU294) interact exclusively with Siponimod.

In the case of S1PR2, S1P interacts strongly with only 8 residues, of which ARG108 uniquely binds to S1P (Figure 3a & 3b). The remaining 7 residues also participate in stabilizing Siponimod at the active site of S1PR2. Moreover, Siponimod engages with an additional 10 residues in S1PR2's active site, including LEU183, PHE86, SER117, ALA112, VAL120, LEU162, PHE198, ILE197, TRP246, and LEU253.

Although the similar set of active site residues contribute towards binding of S1P and Siponimod, the chemical nature of interaction varies between the binding of S1P and Siponimod. While S1P binding to the active site is primarily driven by electrostatic interactions, van der Waals forces play a key role in stabilizing Siponimod. Approximately 55% of Siponimod's binding free energy to S1PR1 (and about 52% to S1PR2) arises from a network of individually weak van der Waals interactions with residues across various secondary structural domains. The most significant contributions come from LEU297 in S1PR1 ($L^{7.39}$) and PHE274 in S1PR2 ($F^{7.39}$), a residue previously believed to hinder Siponimod's binding to the active site of S1PR2. In contrast, a few strong electrostatic interactions (such as ARG120 in S1PR1 and ARG108 in S1PR2) are responsible for anchoring S1P at the active site.

Analysis of pairwise energy decomposition (Figure 3) further suggests that Siponimod's binding profiles to S1PR1 and S1PR2 differ significantly. In S1PR1, nearly 40% of Siponimod's binding free energy stems from its interactions with residues in TM6 and TM7, whereas in S1PR2, this contribution is only about 18%. Among the TM6 and TM7 residues that interact exclusively with Siponimod in S1PR1, LEU272 ($L^{6.51}$) contributes the most (-3.2 kcal/mol). The TM6/TM7

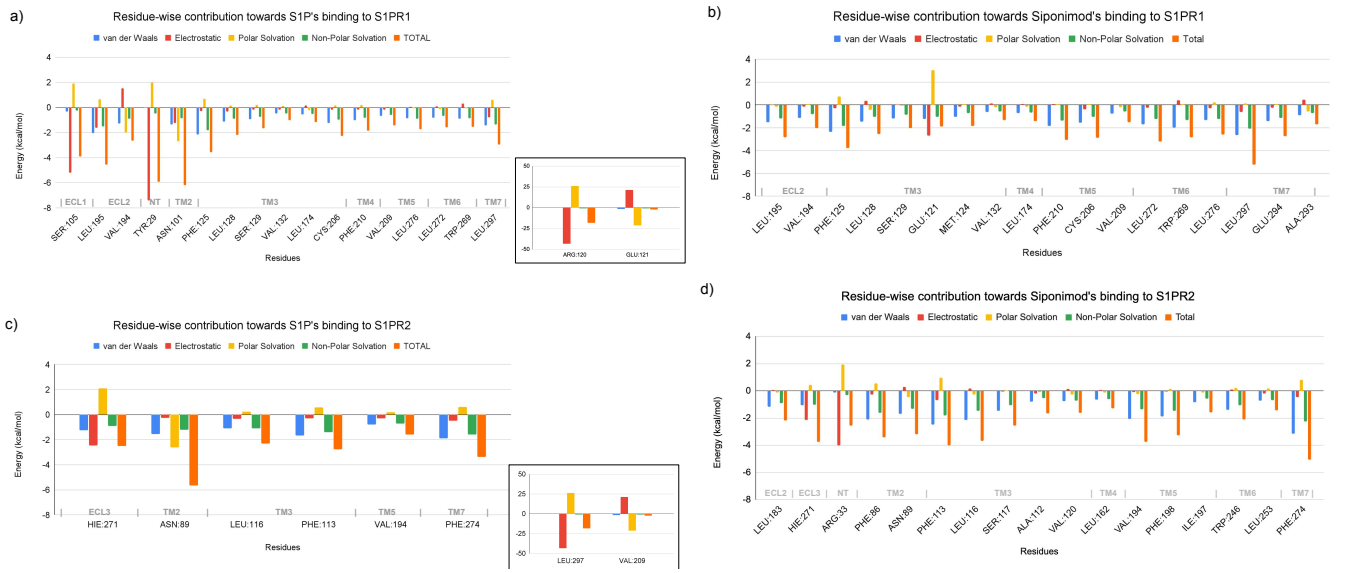

FIG. 3. Residue-wise contribution towards binding free energies of (a) S1P to S1PR1, (b) Siponimod to S1PR1, (c) S1P to S1PR1 and (d) Siponimod to S1PR2, averaged over 2 independent replicas of long ($\approx 1\mu$s each) MD trajectories. Most of the energy components fall within the range of -8 to 4 kcal/mol. Instances where one or more energy components exceed this range are displayed separately in the inset.

residues shared between S1PR1 and S1PR2 include $W^{6.48}$ (part of a key transmission switch, discussed later) and $L^{7.39}$, which is mutated to $F^{7.39}$ in S1PR2. These subtle differences likely contribute to limiting Siponimod's efficacy as a modulator of S1PR2.

E. The binding of Siponimod and S1P differentially influences the structural dynamics of S1PR2

Dynamic cross-correlation maps (DCCM) provide an averaged representation of how each residue moves relative to others throughout the simulation. DCCMs were generated for the HOLO systems taking the entire $\approx 2\mu$s data combining both the replicas (Figure SI 8). Both S1P (Figure SI 8a) and Siponimod (Figure SI 8b) binding to S1PR1 induce similar patterns of correlated and anti-correlated motions across the receptor residues. The only notable difference occurs in the dynamics of the N-terminal (NT) domain. Upon Siponimod binding, the NT residues exhibit correlated movements with residues from the extracellular loops ECL1 and ECL2 (region encircled in orange and brown in Figure SI 8b), whereas these movements are anti-correlated when S1P is bound. However, the DCCMs show two major differences in mutual structural dynamics of S1PR2 residues that is induced by Siponimod binding exclusively. They are discussed in the following sections.

The first difference is observed in the dynamics of the intracellular loops ICL2 and ICL3, regions that interact with the Gα protein in the cytoplasm, with respect to the rest of the protein. ICL3 is the longest cytoplasmic loop in S1PR1, whereas in S1PR2, both ICL2 and ICL3 are of similar length. When S1P binds, the residues of ICL3 (and part of TM6) in S1PR1 (Figure SI 8a, region encircled in grey) and the residues of ICL2 in S1PR2 (Figure SI 8c, region encircled in green) exhibit strong anti-correlated movement with the rest of the receptor. Siponimod binding replicates this anti-correlated dynamic in S1PR1 (Figure SI 8b, region encircled in grey), but fails to induce a comparable effect in S1PR2 (Figure SI 8d, region encircled in green). Hence, although Siponimod binds tightly to the active site, it does not significantly influence the dynamics of the G protein-binding regions in S1PR2.

The second difference is found in the mutual dynamics of transmembrane (TM) helices. When S1P binds to S1PR1 or S1PR2, the TM helices display mostly anti-correlated motions. However, when Siponimod binds to S1PR2, several motion patterns shift, leading to moderately correlated motions, such as between TM6 and TM2 (Figure SI 8d, region encircled in black). The TM2 also shows correlated motions with ICL1 on Siponimod binding (Figure SI 8d, region encircled in magenta). Siponimod binding to S1PR1 does not cause similar changes. These findings highlight the differential impact of Siponimod and S1P binding on S1PR2's dynamic behavior.

F. Key transmission switches remain inactive upon Siponimod binding to S1PR2

Activation of GPCRs, including the five S1P receptor family members, is known to take place through conformational changes of certain residues in the transmembrane helices. These residues are generally referred to as transmission switches[29,65–67]. Through MD simulations, we sought to determine the movements of these transmission switches across apo, S1P-bound and Siponimod-bound receptors, S1PR1 and S1PR2. Analysis of MD trajectories reveal that, compared to S1P, Siponimod leads to a different conformation change in the transmission switches upon binding to S1PR2. The dif-

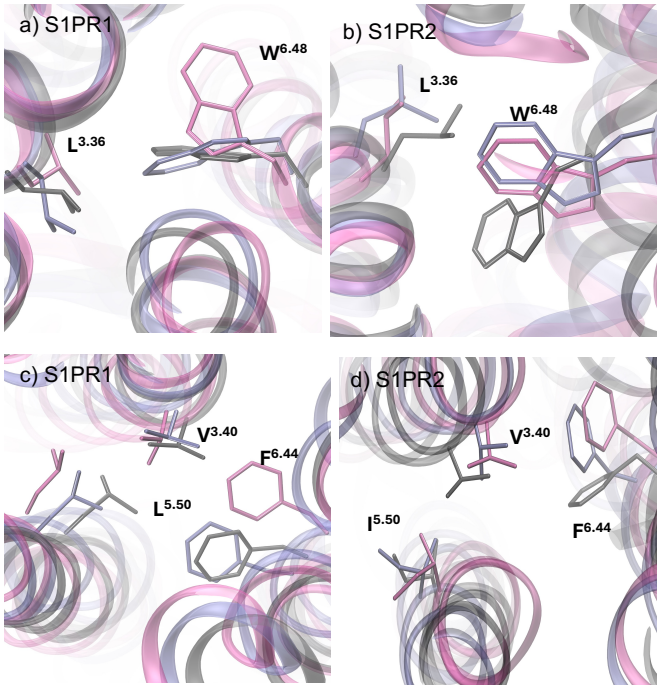

FIG. 4. Transmission switches in S1PR1 and S1PR2. a) $L^{3.36}$-$W^{6.48}$ switches exhibit similar flip in S1P and Siponimod bound S1PR1; b) $L^{3.36}$-$W^{6.48}$ switches exhibit different orientations in S1P and Siponimod bound S1PR2; c) S1P and Siponimod exhibiting similar structural changes in $L^{5.50}$-$V^{3.40}$-$F^{6.44}$ motif in S1PR1; d) S1P and Siponimod exhibiting noticeably different structural changes in $I^{5.50}$-$V^{3.40}$-$F^{6.44}$ motif. Customized Collective Variables (CVs) were used to track the above switching events in the MD trajectories (see Figure SI 9 and SI 10).

ferential influence of S1P and Siponimod binding to the two key transmission switches in S1PRs known to differentiate the active vs inactive conformations are discussed below.

1. $W^{6.48}$ serves as a critical switch in GPCRs, including the S1P receptors, leading to receptor activation upon ligand binding[68,69]. Careful observations of the MD trajectories reveal that the $W^{6.48}$ switch is present in two distinctly different orientations when it is bound to S1P (active mode) vs. when ligand free (inactive mode). In S1PR1, the $W^{6.48}$ switch is found to stay in its active mode during the trajectory when Siponimod is bound (Figure 4a). However, in S1PR2, the $W^{6.48}$ switch is no longer found in its active mode once Siponimod is bound. (Figure 4b). This change in $W^{6.48}$ switch conformation in Siponimod bound S1PR2 resulted in an inward movement of TM6 resulting in a decrease in distance between TM3 and TM6 as evident from the distance between $V^{3.40}$ and $F^{6.44}$ (Figure 5).

2. Another conserved motif, $P^{5.50}$-$I^{3.40}$-$F^{6.44}$, in GPCRs is known to play important role in receptor activation[70,71]. In case of S1PR1 and S1PR2, $L^{5.50}$-$V^{3.40}$-$F^{6.44}$ and $I^{5.50}$-$V^{3.40}$- $F^{6.44}$ motifs, respectively, play a similar role[72]. Similar to the $W^{6.48}$ switch, the $L^{5.50}$-$V^{3.40}$-$F^{6.44}$ switch in S1PR1 and the $I^{5.50}$-$V^{3.40}$-$F^{6.44}$ switch in S1PR2, are present in two distinctly different orientations when they are bound to S1P (active mode) vs. when ligand free (inactive mode). In S1PR1, the $L^{5.50}$-$V^{3.40}$-$F^{6.44}$ switch is maintaining its active mode (marked by $F^{6.44}$ and $V^{3.40}$ orientations) when Siponimod is bound (Figure 4c). However, in S1PR2, the $I^{5.50}$-$V^{3.40}$-$F^{6.44}$ switch could not retain its active mode (marked by a shift in $F^{6.44}$ orientations) on Siponimod binding (Figure 4d).

The DCCMs reveal that TM6 residues exhibit distinct motion in S1PR2 when Siponimod is bound, in contrast to the S1P-bound state (Figure SI 8). Porcupine plots obtained from PCA of the MD trajectories (Figure SI 7) suggests that in response to S1P binding at the active site, TM6 and TM7 move away from each other in opposite directions in both S1PR1 and S1PR2. On Siponimod binding, similar movements of TM6 and TM7 residues are observed in S1PR1, but not in S1PR2. In S1PR2 they move close to each other. This divergence is likely due to Siponimod forming minimal strong interactions with TM6 and TM7 residues at the active site of S1PR2 (Figure 3). The relative movements of TM6 and TM7 in S1P receptors are closely linked to receptor activation[17,73]. Our analysis shows that ligand binding triggers significant conformational changes in key residues, particularly $F^{6.44}$ and $V^{3.40}$. These shifts, coupled with movements in $W^{6.48}$ and $L^{3.36}$, play a crucial role in regulating the relative positioning of the transmembrane helices, which ultimately influences receptor activation dynamics.

So, a similar transmission switch dynamics is observed when Siponimod binds to S1PR1, but not when it binds to S1PR2 as compared to their respective S1P counterparts. Given that the MD simulations were initiated from an active state conformation of the receptors, this implies that Siponimod binding at the active site of S1PR2 is not able to hold the active state conformation of S1PR2. The relative positioning of key transmembrane helices, specifically TM6 and TM7, was analyzed in relation to the known inactive conformation of S1PR1 (PDB ID: 3V2Y[74]). The last frames from the two MS simulation replicas were overlaid onto the inactive S1PR1 conformation (Figure 5). It is evident that S1PR2 resembles the inactive state conformation (pink structure in Figure 5b) when it is bound to Siponimod (blue structure in Figure 5b). S1P bound S1PR2 conformation is distinctly different.

In addition to the transmission switches mentioned earlier, significant differences in the conformation of residues near the extracellular region of TM7 were observed between S1P-bound and Siponimod-bound S1PR2. These differences are mainly driven by the dynamics of H^{ECL3}, $Y^{7.37}$, $F^{7.38}$, and $F^{7.39}$ in the TM7 helix. Although the orientation of these residues varies slightly between the two replicas, the relative positioning of H^{ECL3} and $F^{7.39}$ remains consistent (Figure SI 11). Notably, these residues are absent in S1PR1, as discussed earlier. It appears that conformational changes in H^{ECL3} and the associated residues ($Y^{7.37}$, $F^{7.38}$, and $F^{7.39}$) contribute to S1PR2 activation upon S1P binding, but not with Siponimod binding.

Previous studies have also shown that $PHE^{7.39}$ in S1PR2 plays a role in its selectivity towards the inhibitor JTE-013.

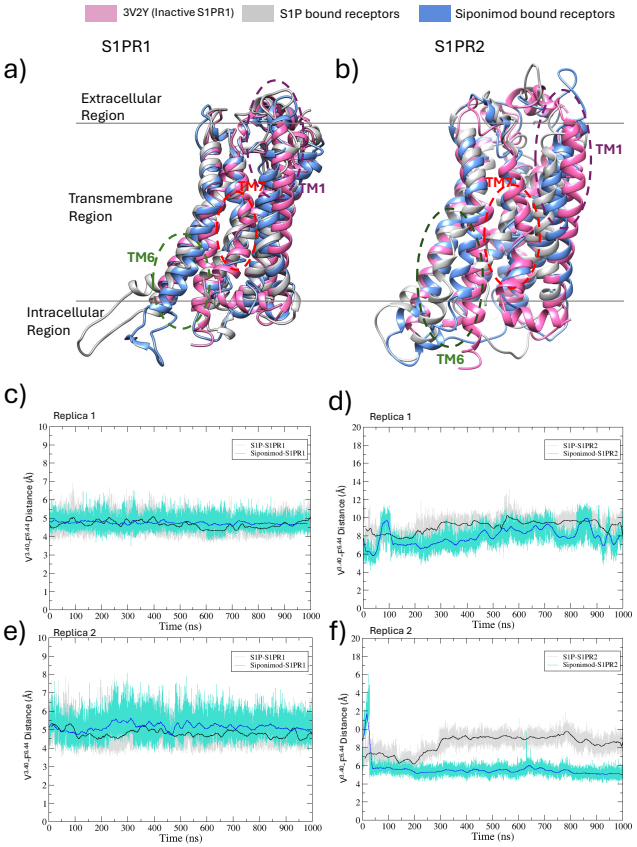

FIG. 5. In panels (a) and (b), we compare the S1P- and Siponimod-bound conformations of S1PR1 and S1PR2 with the inactive S1PR1 structure. Panels (c) and (e) show the distance changes between helices TM3 and TM6 for S1PR1 across both replicas, while panels (d) and (f) show the same for S1PR2. In S1PR1, TM6 remains mostly outward in both the S1P- and Siponimod-bound states. However, in Siponimod-bound S1PR2, the distance between TM3 and TM6 decreases due to TM6 moving inward. TM6 tends to move inward in Siponimod-bound S1PR2 but stays outward in S1P-bound S1PR2. The distance between TM3 and TM6 remains consistent in both S1P-bound S1PR1 and S1PR2, as well as in Siponimod-bound S1PR1.

Specifically, the mutation F274I reduced the receptor's response to JTE-013 but enhanced downstream activity upon binding to FTY720-P[17]. Thus, we hypothesize that PHE$^{7.39}$, along with HIS^{ECL3} and TYR$^{7.37}$, could be critical in designing selective modulators for S1P receptors. Another key residue in this context is L$^{6.51}$, which makes the largest contribution to Siponimod's binding to S1PR1 but does not interact with Siponimod in S1PR2. These residues could be targeted to optimize molecules for either enhanced or reduced binding to S1PR2, depending on therapeutic requirements.

IV. CONCLUSION

Drug candidates can be optimized to address target selectivity on the grounds of shape of binding pockets, electrostatic properties on binding ligand, flexibility of residues inside pocket, hydration behavior of target protein, and allosteric inhibition[75]. Modifying the drug candidates to selectivity fit the target protein becomes increasingly intricate when dealing with targets and off-targets within same sub-family of proteins with significant amount of structural and sequence homology as observed in S1P receptors in this study. For large proteins such as GPCRs, although the scientific community is looking into allosteric modulators[76], discerning druggable metastable states or pinpointing effective allosteric pockets can be challenging.

Through this work we suggest utilizing computational methods like molecular docking and MD simulations to a) assess the binding strength of ligands inside protein pockets, b) understand the chemical nature of protein-ligand interactions and c) delineate the influence of ligand binding on the structural dynamics of the protein. In this study, we successfully demonstrated that, a strong ligand binding does not necessarily transfer to biological activity and MD simulations can shed more light on the induced structural changes required for target activity. In particular, we demonstrate that Siponimod binds strongly to the active site of S1PR2, but fails to trigger the conformational changes in the W$^{6.48}$ and the I$^{5.50}$-V$^{3.40}$-F$^{6.44}$ transmission switches, which are essential for the rearrangement of the transmembrane helices TM6 and TM7 required to activate the receptor.

For further validating our hypothesis we propose performing radioligand competitive binding assays to confirm Siponimod's binding to S1PR2. Note that, similar assays have already been performed to check Siponimod's binding to other S1PRs (S1PR1 and S1PR5)[27]. Also enhanced MD simulations designed to study the ligand binding/unbinding kinetics can estimate the residence time of ligand in the protein pocket. Binding affinities, as obtained from conventional MD simulations performed in this work, when combined with the residence time details of the ligand can discern more accurate picture of protein-ligand interactions[77]. Such studies are beyond the scope of the present work. Nevertheless, with our current exercise we were able to leverage MD to compare the structural dynamics of the receptors, S1PR1 and S1PR2, when bound to S1P and Siponimod. We could infer that the structural dynamics of S1PR1 were similarly affected by both S1P and Siponimod binding, whereas S1PR2 responded differently to the binding of these two molecules. We could also observe that lack of strong interactions between Siponimod and residues of TM6 and TM7 was responsible for the difference in dynamics. We propose that avoiding interactions with TM6 and TM7 residues in S1PR2 can be exploited to design selective modulators for S1P receptors. We could also observe that interaction of HIS^{ECL3}(HIS271) with Siponimod in S1PR2 was responsible for the difference in dynamics. We propose that three residues, PHE$^{7.39}$, HIS^{ECL3} and TYR$^{7.37}$, can be exploited to design selective modulators for S1P receptors.

SUPPORTING INFORMATION

See the "Supporting Information" material for Figure SI 1 - Figure SI 11, details of MD protocol used, sequence alignment of S1PR1 with respect to S1PR2 and annotation of the residues important for their activation mechanism, S1PR1 and S1PR2 structure alignment using Foldseek, aligning docked pose of Siponimod to Siponimod in experimentally available S1PR1, assessing system fluctuations via RMSD and RMSF analysis of MD trajectories, principal component analysis of the MD trajectories, details of the step-wise protocol used to consolidate the residue-wise energy contribution data, analyzing inter-residue dynamics using dynamic cross-correlation maps, changes in transmission switches on ligand binding in S1PR1 and S1PR2.

ACKNOWLEDGMENTS

We appreciate the contribution of Toran Roy and Srinivas Tumuluri in the initial discussions on the peoject. We are grateful to Dr. Shubhandra Tripathi, Dr. Madhura Mohole, Dr. Srinath V. K. Kompella, Prasad Chodavarapu and Vikram Duvvoori for the invaluable discussions and constructive feedback during the preparation of manuscript.

DATA AVAILABILITY STATEMENT

PDB IDs for protein files used in the article are mentioned in main manuscript. MD simulation data can be made available on request.

AUTHOR DECLARATIONS

Conflict of Interest

All the authors are the employees of Aganitha.ai, the company that holds interests in any commercial gains arising out of this work.

Author contributions

Kumari Soniya: Formal analysis (lead); Investigation (lead); Writing - original draft (lead); Writing – review & editing (equal). **Chanukya Nanduru**: Supervision (lead); Writing – review & editing (equal). **Antarip Halder**: Conceptualization (lead); Formal analysis (supporting); Writing – review & editing (equal).

[1] S. Saikia, M. Bordoloi, and R. Sarmah, "Established and in-trial GPCR families in clinical trials: A review for target selection," *Curr. Drug Targets* **20** (2018), 10.2174/1389450120666181105152439.

[2] K. Sriram and P. A. Insel, "G protein-coupled receptors as targets for approved drugs: How many targets and how many drugs?" *Mol. Pharmacol.* **93** (2018), 10.1124/mol.117.111062.

[3] A. S. Hauser, M. M. Attwood, M. Rask-Andersen, H. B. Schiöth, and D. E. Gloriam, "Trends in gpcr drug discovery: New agents, targets and indications," *Nat. Rev. Drug Discov.* **16** (2017), 10.1038/nrd.2017.178.

[4] T. Laeremans, Z. A. Sands, P. Claes, A. D. Blieck, S. D. Cesco, S. Triest, A. Busch, D. Felix, A. Kumar, V. P. Jaakola, and C. Menet, "Accelerating GPCR drug discovery with conformation-stabilizing VHHs," *Front. Mol. Biosci.* **9** (2022), 10.3389/fmolb.2022.863099.

[5] D. Yang, Q. Zhou, V. Labroska, S. Qin, S. Darbalaei, Y. Wu, E. Yuliantie, L. Xie, H. Tao, J. Cheng, Q. Liu, S. Zhao, W. Shui, Y. Jiang, and M. W. Wang, "G protein-coupled receptors: structure- and function-based drug discovery," *Signal. Transduct. Target. Ther.* **6** (2021), 10.1038/s41392-020-00435-w.

[6] K. Mendelson, T. Evans, and T. Hla, "Sphingosine 1-phosphate signalling," *Dev. (Camb.)* **141** (2014), 10.1242/dev.094805.

[7] J. G. Cyster and S. R. Schwab, "Sphingosine-1-phosphate and lymphocyte egress from lymphoid organs," *Annu. Rev. Immunol.* **30** (2012), 10.1146/annurev-immunol-020711-075011.

[8] R. Pappu, S. R. Schwab, I. Cornelissen, J. P. Pereira, J. B. Regard, Y. Xu, E. Camerer, Y. W. Zheng, Y. Huang, J. G. Cyster, and S. R. Coughlin, "Promotion of lymphocyte egress into blood and lymph by distinct sources of sphingosine-1-phosphate," *Science* **316** (2007), 10.1126/science.1139221.

[9] G. Álvarez Bravo, R. R. Cedeño, M. P. Casadevall, and L. Ramió-Torrentà, "Sphingosine-1-phosphate (S1P) and S1P signaling pathway modulators, from current insights to future perspectives," *Cells* **11** (2022), 10.3390/cells11132058.

[10] R. Roy, A. A. Alotaibi, and M. S. Freedman, "Sphingosine 1-phosphate receptor modulators for multiple sclerosis," *CNS Drugs* **35** (2021), 10.1007/s40263-021-00798-w.

[11] O. J. Kandjani, S. Yaqoubi, S. S. Vahdati, B. Borhannejad, S. Dastmalchi, and A. A. Alizadeh, "S1PR1 modulators in multiple sclerosis: Efficacy, safety, comparison, and chemical structure insights," *Eur. J. Med. Chem.* **250** (2023), 10.1016/j.ejmech.2023.115182.

[12] P. K. Coyle, M. S. Freedman, B. A. Cohen, B. A. Cree, and C. E. Markowitz, "Sphingosine 1-phosphate receptor modulators in multiple sclerosis treatment: A practical review," *Ann. Clin. Transl. Neurol.* **11** (2024), 10.1002/acn3.52017.

[13] Y. Liu, Y. Zhi, H. Song, M. Zong, J. Yi, G. Mao, L. Chen, and G. Huang, "S1PR1 promotes proliferation and inhibits apoptosis of esophageal squamous cell carcinoma through activating STAT3 pathway," *J. Exp. Clin. Cancer Res.* **38** (2019), 10.1186/s13046-019-1369-7.

[14] M. Hao, R. Fu, J. Tai, Z. Tian, X. Yuan, Y. Chen, M. Wang, H. Jiang, M. Ji, F. Lai, N. Xue, L. Bai, Y. Zhu, X. Lv, X. Chen, and J. Jin, "S1PR1 serves as a viable drug target against pulmonary fibrosis by increasing the integrity of the endothelial barrier of the lung," *Acta Pharm. Sin. B.* **13** (2023), 10.1016/j.apsb.2022.10.006.

[15] V. Constantinescu, R. Haase, K. Akgün, and T. Ziemssen, "S1p receptor modulators and the cardiovascular autonomic nervous system in multiple sclerosis: a narrative review," *Ther. Adv. Neurol. Disord.* **15** (2022), 10.1177/17562864221133163.

[16] D. Mazurais, P. Robert, B. Gout, I. Berrebi-Bertrand, M. P. Laville, and T. Calmels, "Cell type-specific localization of human cardiac s1p receptors," *J. Histochem. Cytochem.* **50** (2002), 10.1177/002215540205000507.

[17] H. Chen, K. Chen, W. Huang, L. M. Staudt, J. G. Cyster, and X. Li, "Structure of s1pr2–heterotrimeric g13 signaling complex," *Sci. Adv.* **8** (2022), 10.1126/sciadv.abn0067.

[18] M. Pang, C. Li, D. Zheng, Y. Wang, J. Wang, W. Zhang, F. Li, and H. Jing, "S1PR2 knockdown promotes migration and invasion in multiple myeloma cells via NF-κB activation," *Cancer Manag. Res.* **12** (2020), 10.2147/CMAR.S237330.

[19] S. Mandala, R. Hajdu, J. Bergstrom, E. Quackenbush, J. Xie, J. Milligan, R. Thornton, G. J. Shei, D. Card, C. A. Keohane, M. Rosenbach, J. Hale, C. L. Lynch, K. Rupprecht, W. Parsons, and H. Rosen, "Alteration of lymphocyte trafficking by sphingosine-1-phosphate receptor agonists," *Science* **296** (2002), 10.1126/science.1070238.

[20] J. Chun and H. P. Hartung, "Mechanism of action of oral fingolimod (FTY720) in multiple sclerosis," *Clin. Neuropharmacol.* **33** (2010), 10.1097/WNF.0b013e3181cbf825.

[21] L. Kappos, J. Antel, G. Comi, X. Montalban, P. O'Connor, C. H. Polman, T. Haas, A. A. Korn, G. Karlsson, and E. W. Radue, "Oral fingolimod (FTY720) for relapsing multiple sclerosis," *N. Engl. J. Med.* **355** (2006),

10.1056/nejmoa052643.

[22]P. Gergely, B. Nuesslein-Hildesheim, D. Guerini, V. Brinkmann, M. Traebert, C. Bruns, S. Pan, N. S. Gray, K. Hinterding, N. G. Cooke, A. Groenewegen, A. Vitaliti, T. Sing, O. Luttringer, J. Yang, A. Gardin, N. Wang, W. J. Crumb, M. Saltzman, M. Rosenberg, and E. Wallström, "The selective sphingosine 1-phosphate receptor modulator BAF312 redirects lymphocyte distribution and has species-specific effects on heart rate," *Br. J. Pharmacol.* **167** (2012), 10.1111/j.1476-5381.2012.02061.x.

[23]C. Harrison and J. R. Traynor, "The [^{35}S]GTPγS binding assay: Approaches and applications in pharmacology," *Life Sci.* **74** (2003), 10.1016/j.lfs.2003.07.005.

[24]D. Hilger, M. Masureel, and B. K. Kobilka, "Structure and dynamics of GPCR signaling complexes," *Nat. Struct. Mol. Biol.* **25** (2018), 10.1038/s41594-017-0011-7.

[25]L. Kappos, A. Bar-Or, B. A. Cree, R. J. Fox, G. Giovannoni, R. Gold, P. Vermersch, D. L. Arnold, S. Arnould, T. Scherz, C. Wolf, E. Wallström, F. Dahlke, A. Achiron, L. Achtnichts, K. Agan, G. Akman-Demir, A. B. Allen, J. P. Antel, A. R. Antiguedad, M. Apperson, A. M. Applebee, G. I. Ayuso, M. Baba, O. Bajenaru, R. Balasa, B. P. Balci, M. Barnett, A. Bass, V. U. Becker, M. Bejinariu, F. T. Bergh, A. Bergmann, E. Bernitsas, A. Berthele, V. Bhan, F. Bischof, R. J. Bjork, G. Blevins, M. Boehringer, T. Boerner, R. Bonek, J. D. Bowen, A. Bowling, A. N. Boyko, C. Boz, V. Bracknies, S. Braune, V. B. Morra, B. Brochet, W. Brola, P. K. Brownstone, M. Brozman, D. Brunet, I. Buraga, M. Burnett, M. Buttmann, H. Butzkueven, J. Cahill, J. C. Calkwood, W. Camu, M. Cascione, G. Castelnovo, D. Centonze, J. Cerqueira, A. Chan, A. Cimprichova, S. Cohan, G. Comi, J. Conway, J. A. Cooper, J. Corboy, J. Correale, B. Costell, D. A. Cottrell, P. K. Coyle, M. Craner, L. Cui, L. Cunha, A. Czlonkowska, A. M. da Silva, J. de Sa, J. de Seze, M. Debouverie, J. Debruyne, D. Decoo, G. Defer, T. Derfuss, N. H. Deri, B. Dihenia, P. Dioszeghy, V. Donath, B. Dubois, M. Duddy, P. Duquette, G. Edan, H. Efendi, S. Elias, P. J. Emrich, B. C. Estruch, E. P. Evdoshenko, J. Faiss, A. S. Fedyanin, W. Feneberg, J. Fermont, O. F. Fernandez, F. C. Ferrer, K. Fink, H. Ford, C. Ford, A. Francia, M. Freedman, B. Frishberg, S. Galgani, G. P. Garmany, K. Gehring, J. Gitt, C. Gobbi, L. P. Goldstick, R. A. Gonzalez, F. Grandmaison, N. Grigoriadis, O. Grigorova, L. M. E. Grimaldi, J. Gross, K. Gross-Paju, M. Gudesblatt, D. Guillaume, J. Haas, V. Hancinova, A. Hancu, O. Hardiman, A. Harmjanz, F. R. Heidenreich, G. J. Hengstman, J. Herbert, M. Herring, S. Hodgkinson, O. M. Hoffmann, W. E. Hofmann, W. D. Honeycutt, L. H. Hua, D. Huang, Y. Huang, D. R. Huang, R. Hupperts, P. Imre, A. K. Jacobs, G. Jakab, E. Jasinska, K. Kaida, J. Kalnina, A. Kaprelyan, G. Karelis, D. Karussis, A. Katz, F. A. Khabirov, B. Khatri, T. Kimura, I. Kister, R. Kizlaitiene, E. Klimova, J. Koehler, A. Komatineni, A. Kornhuber, K. Kovacs, A. Koves, W. Kozubski, G. Krastev, L. B. Krupp, E. Kurca, C. Lassek, G. Laureys, L. Lee, E. Lensch, F. Leutmezer, H. Li, R. A. Linker, M. Linnebank, P. Liskova, C. Llanera, J. Lu, A. Lutterotti, J. Lycke, R. Macdonell, M. Maciejowski, M. Maeurer, R. V. Magzhanov, E. M. Maida, L. Malciene, Y. Mao-Draayer, G. A. Marfia, C. Markowitz, V. Mastorodimos, K. Matyas, J. Meca-Lallana, J. A. G. Merino, I. G. Mihetiu, I. Milanov, A. E. Miller, A. Millers, M. Mirabella, M. Mizuno, X. Montalban, L. Montoya, M. Mori, S. Mueller, J. Nakahara, Y. Nakatsuji, S. Newsome, R. Nicholas, A. S. Nielsen, E. Nikfekr, U. Nocentini, C. Nohara, K. Nomura, M. M. Odinak, T. Olsson, B. W. van Oosten, C. Oreja-Guevara, P. Oschmann, J. Overell, A. Pachner, G. Panczel, M. Pandolfo, C. Papeix, L. Patrucco, J. Pelletier, R. Piedrabuena, M. Pless, U. Polzer, K. Pozsegovits, D. Rastenyte, S. Rauer, G. Reifschneider, R. Rey, S. A. Rizvi, D. Robertson, J. M. Rodriguez, D. Rog, H. Roshanisefat, V. Rowe, C. Rozsa, S. Rubin, S. Rusek, F. Saccà, T. Saida, A. V. Salgado, V. E. F. Sanchez, K. Sanders, M. Satori, D. V. Sazonov, E. A. Scarpini, E. Schlegel, M. Schluep, S. Schmidt, E. Scholz, H. M. Schrijver, M. Schwab, R. Schwartz, J. Scott, K. Selmaj, S. Shafer, B. Sharrack, I. A. Shchukin, Y. Shimizu, P. Shotekov, A. Siever, K. O. Sigel, S. Silliman, M. Simo, M. Simu, V. Sinay, A. E. Siquier, A. Siva, O. Skoda, A. Solomon, M. Stangel, D. Stefoski, B. Steingo, I. D. Stolyarov, P. Stourac, K. Strassburger-Krogias, E. Strauss, O. Stuve, I. Tarnev, A. Tavernarakis, C. R. Tello, M. Terzi, V. Ticha, M. Ticmeanu, K. Tiel-Wilck, T. Toomsoo, N. Tubridy, M. J. Tullman, H. Tumani, P. Turcani, B. Turner, A. Uccelli, F. J. O. Urtaza, M. Vachova, A. Valikovics, S. Walter, B. V. Wijmeersch, L. Vanopdenbosch, J. R. Weber, S. Weiss, R. Weissert, P. Vermersch, T. West, H. Wiendl, S. Wiertlewski, B. Wildemann, B. Willekens, L. H. Visser, G. Vorobeychik, X. Xu, T. Yamamura, Y. N. Yang, S. M. Yelamos, M. Yeung, A. Zacharias, M. Zelkowitz, U. Zettl, M. Zhang, H. Zhou, U. Zieman, and T. Ziemssen, "Siponimod versus placebo in secondary progressive multiple sclerosis (EXPAND): a double-blind, randomised, phase 3 study," *The Lancet.* **391** (2018), 10.1016/S0140-6736(18)30475-6.

[26]E. R. Hammond, "Perspectives on safety and efficacy-the BOLD phase 2 extension study of siponimod in relapsing-remitting multiple sclerosis," *JAMA Neurol.* **73** (2016), 10.1001/jamaneurol.2016.2284.

[27]J. V. Selkirk, A. Bortolato, Y. G. Yan, N. Ching, and R. Hargreaves, "Competitive binding of ozanimod and other sphingosine 1-phosphate receptor modulators at receptor subtypes 1 and 5," *Front. Pharmacol.* **13** (2022), 10.3389/fphar.2022.892097.

[28]V. T. Sabe, T. Ntombela, L. A. Jhamba, G. E. Maguire, T. Govender, T. Naicker, and H. G. Kruger, "Current trends in computer aided drug design and a highlight of drugs discovered via computational techniques: A review," *Eur. J. Med. Chem.* **224** (2021), 10.1016/j.ejmech.2021.113705.

[29]S. Liu, N. Paknejad, L. Zhu, Y. Kihara, M. Ray, J. Chun, W. Liu, R. K. Hite, and X. Y. Huang, "Differential activation mechanisms of lipid GPCRs by lysophosphatidic acid and sphingosine 1-phosphate," *Nat. Commun.* **13** (2022), 10.1038/s41467-022-28417-2.

[30]A. Jacob, J. Lancaster, J. Buhler, B. Harris, and R. D. Chamberlain, "Mercury BLASTP: Accelerating protein sequence alignment," *ACM Trans. Reconfigurable Technol. Syst.* **1** (2008), 10.1145/1371579.1371581.

[31]A. Mahram and M. C. Herbordt, "NCBI BLASTP on high-performance reconfigurable computing systems," *ACM Trans. Reconfigurable Technol. Syst.* **7** (2015), 10.1145/2629691.

[32]J. A. Ballesteros and H. Weinstein, "[19] integrated methods for the construction of three-dimensional models and computational probing of structure-function relations in g protein-coupled receptors," (Academic Press, 1995) pp. 366–428.

[33]F. Horn, J. Weare, M. W. Beukers, S. Hörsch, A. Bairoch, W. Chen, Edvardsen, F. Campagne, and G. Vriend, "GPCRDB: An information system for g protein-coupled receptors," *Nucleic Acids Res.* **26** (1998), 10.1093/nar/26.1.275.

[34]G. Pándy-Szekeres, J. Caroli, A. Mamyrbekov, A. A. Kermani, G. M. Keseru, A. J. Kooistra, and D. E. Gloriam, "GPCRdb in 2023: state-specific structure models using AlphaFold2 and new ligand resources," *Nucleic Acids Res.* **51** (2023), 10.1093/nar/gkac1013.

[35]A. Waterhouse, M. Bertoni, S. Bienert, G. Studer, G. Tauriello, R. Gumienny, F. T. Heer, T. A. D. Beer, C. Rempfer, L. Bordoli, R. Lepore, and T. Schwede, "SWISS-MODEL: Homology modelling of protein structures and complexes," *Nucleic Acids Res.* **46** (2018), 10.1093/nar/gky427.

[36]M. van Kempen, S. S. Kim, C. Tumescheit, M. Mirdita, J. Lee, C. L. Gilchrist, J. Söding, and M. Steinegger, "Fast and accurate protein structure search with foldseek," *Nat. Biotechnol.* **42** (2024), 10.1038/s41587-023-01773-0.

[37]Y. Zhang and J. Skolnick, "Scoring function for automated assessment of protein structure template quality," *Proteins: Struct. Funct. Genet.* **57** (2004), 10.1002/prot.20264.

[38]J. Eberhardt, D. Santos-Martins, A. F. Tillack, and S. Forli, "AutoDock Vina 1.2.0: new docking methods, expanded force field, and python bindings," *J. Chem. Inf. Model.* **61** (2021), 10.1021/acs.jcim.1c00203.

[39]S. Tang, R. Chen, M. Lin, Q. Lin, Y. Zhu, J. Ding, H. Hu, M. Ling, and J. Wu, "Accelerating AutoDock vina with GPUs," *Molecules* **27** (2022), 10.3390/molecules27093041.

[40]E. F. Pettersen, T. D. Goddard, C. C. Huang, G. S. Couch, D. M. Greenblatt, E. C. Meng, and T. E. Ferrin, "UCSF Chimera - a visualization system for exploratory research and analysis," *J. Comput. Chem.* **25** (2004), 10.1002/jcc.20084.

[41]S. Salentin, S. Schreiber, V. J. Haupt, M. F. Adasme, and M. Schroeder, "PLIP: Fully automated protein-ligand interaction profiler," *Nucleic Acids Res.* **43** (2015), 10.1093/nar/gkv315.

[42]D. A. Case, H. M. Aktulga, K. Belfon, I. Y. Ben-Shalom, J. T. Berryman, S. R. Brozell, D. S. Cerutti, T. E. C. III, G. A. Cisneros, V. W. D. Cruzeiro, T. A. Darden, N. Forouzesh, G. Giambaşu, T. Giese, M. K. Gilson, H. Gohlke, A. W. Goetz, J. Harris, S. Izadi, S. A. Izmailov, K. Kasavajhala, M. C. Kaymak, E. King, A. Kovalenko, T. Kurtzman, T. S. Lee, P. Li, C. Lin, J. Liu, T. Luchko, R. Luo, M. Machado, V. Man, M. Manathunga, K. M. Merz, Y. Miao, O. Mikhailovskii, G. Monard, H. Nguyen, K. A. O'Hearn, A. Onufriev, F. Pan, S. Pantano, R. Qi, A. Rahnamoun,

D. R. Roe, A. Roitberg, C. Sagui, S. Schott-Verdugo, A. Shajan, J. Shen, C. L. Simmerling, N. R. Skrynnikov, J. Smith, J. Swails, R. C. Walker, J. Wang, J. Wang, H. Wei, X. Wu, Y. Wu, Y. Xiong, Y. Xue, D. M. York, S. Zhao, Q. Zhu, and P. A. Kollman, *Amber 2022* (2022).

[43]A. Jakalian, B. L. Bush, D. B. Jack, and C. I. Bayly, "Fast, efficient generation of high-quality atomic charges. AM1-BCC Model: I. method," *J. Comput. Chem.* **21** (2000), 10.1002/(SICI)1096-987X(20000130)21:2<132::AID-JCC5>3.0.CO;2-P.

[44]A. Jakalian, D. B. Jack, and C. I. Bayly, "Fast, efficient generation of high-quality atomic charges. aM1-BCC model: II. parameterization and validation," *J. Comput. Chem.* **23** (2002), 10.1002/jcc.10128.

[45]J. Wang, R. M. Wolf, J. W. Caldwell, P. A. Kollman, and D. A. Case, "Development and testing of a general amber force field," *J. Comput. Chem.* **25** (2004), 10.1002/jcc.20035.

[46]J. Wang, W. Wang, P. A. Kollman, and D. A. Case, "Automatic atom type and bond type perception in molecular mechanical calculations," *J. Mol. Graph. Model.* **25** (2006), 10.1016/j.jmgm.2005.12.005.

[47]S. Schott-Verdugo and H. Gohlke, "PACKMOL-Memgen: A simple-to-use, generalized workflow for membrane-protein-lipid-bilayer system building," *J. Chem. Inf. Model.* **59** (2019), 10.1021/acs.jcim.9b00269.

[48]C. J. Dickson, R. C. Walker, and I. R. Gould, "Lipid21: Complex lipid membrane simulations with AMBER," *J. Chem. Theory Comput.* **18** (2022), 10.1021/acs.jctc.1c01217.

[49]H. J. Berendsen, J. R. Grigera, and T. P. Straatsma, "The missing term in effective pair potentials," *J. Phys. Chem.* **91** (1987), 10.1021/j100308a038.

[50]K. Takemura and A. Kitao, "Effects of water model and simulation box size on protein diffusions motions," *J. Phys. Chem. B.* **111** (2007), 10.1021/jp0756247.

[51]P. Bauer, B. Hess, and E. Lindahl, "GROMACS 2022.3 source code," (2022).

[52]H. J. Berendsen, D. van der Spoel, and R. van Drunen, "GROMACS: A message-passing parallel molecular dynamics implementation," *Comput. Phys. Commun.* **91** (1995), 10.1016/0010-4655(95)00042-E.

[53]H. Bekker, H. Berendsen, E. Dijkstra, S. Achterop, R. v. Vondrumen, D. Vanderspoel, A. Sijbers, H. Keegstra, and M. Renardus, English"GROMACS - a paralel computer for molecular-dynamics simulations," in English*PHYSICS COMPUTING '92*, edited by R. DeGroot and J. Nadrchal (World Scientific Publishing, 1993) pp. 252–256, 4th International Conference on Computational Physics (PC 92) ; Conference date: 24-08-1992 Through 28-08-1992.

[54]W. Humphrey, A. Dalke, and K. Schulten, "VMD: Visual molecular dynamics," *J. Mol. Graph.* **14** (1996), 10.1016/0263-7855(96)00018-5.

[55]K. Pearson, "LIII. on lines and planes of closest fit to systems of points in space," *Lond. Edinb. Dubl. Phil. Mag* **2** (1901), 10.1080/14786440109462720.

[56]D. R. Roe and T. E. Cheatham, "PTRAJ and CPPTRAJ: Software for processing and analysis of molecular dynamics trajectory data," *J. Chem. Theory Comput.* **9** (2013), 10.1021/ct400341p.

[57]B. R. Miller, T. D. McGee, J. M. Swails, N. Homeyer, H. Gohlke, and A. E. Roitberg, "MMPBSA.py: An efficient program for end-state free energy calculations," *J. Chem. Theory Comput.* **8**, 3314–3321 (2012).

[58]M. S. Valdés-Tresanco, M. E. Valdés-Tresanco, P. A. Valiente, and E. Moreno, "Gmx$_{MMPBSA}$: A new tool to perform end-state free energy calculations with GROMACS," *J. Chem. Theory Comput.* **17** (2021), 10.1021/acs.jctc.1c00645.

[59]A. Onufriev, D. Bashford, and D. A. Case, "Exploring protein native states and large-scale conformational changes with a modified generalized born model," *Proteins: Struct., Funct., Bioinf.* **55** (2004), 10.1002/prot.20033.

[60]G. Corso, H. Stärk, B. Jing, R. Barzilay, and T. Jaakkola, "Diffdock: Diffusion steps, twists, and turns for molecular docking," (2023), arXiv:2210.01776 [q-bio.BM].

[61]H. Cai, C. Shen, T. Jian, X. Zhang, T. Chen, X. Han, Z. Yang, W. Dang, C.-Y. Hsieh, Y. Kang, P. Pan, X. Ji, J. Song, T. Hou, and Y. Deng, "Carsidock: a deep learning paradigm for accurate protein–ligand docking and screening based on large-scale pre-training," *Chem. Sci.* **15**, 1449–1471 (2024).

[62]T. K. Sheils, S. L. Mathias, K. J. Kelleher, V. B. Siramshetty, D. T. Nguyen, C. G. Bologa, L. J. Jensen, D. Vidović, A. Koleti, S. C. Schürer, A. Waller, J. J. Yang, J. Holmes, G. Bocci, N. Southall, P. Dharkar, E. Mathé, A. Simeonov, and T. I. Oprea, "TCRD and pharos 2021: Mining the human proteome for disease biology," *Nucleic Acids Res.* **49** (2021), 10.1093/nar/gkaa993.

[63]D. T. Nguyen, S. Mathias, C. Bologa, S. Brunak, N. Fernandez, A. Gaulton, A. Hersey, J. Holmes, L. J. Jensen, A. Karlsson, G. Liu, A. Ma'ayan, G. Mandava, S. Mani, S. Mehta, J. Overington, J. Patel, A. D. Rouillard, S. Schürer, T. Sheils, A. Simeonov, L. A. Sklar, N. Southall, O. Ursu, D. Vidovic, A. Waller, J. Yang, A. Jadhav, T. I. Oprea, and R. Guha, "Pharos: Collating protein information to shed light on the druggable genome," *Nucleic Acids Res.* **45** (2017), 10.1093/nar/gkw1072.

[64]K. J. Kelleher, T. K. Sheils, S. L. Mathias, J. J. Yang, V. T. Metzger, V. B. Siramshetty, D. T. Nguyen, L. J. Jensen, D. Vidović, S. C. Schürer, J. Holmes, K. R. Sharma, A. Pillai, C. G. Bologa, J. S. Edwards, E. A. Mathe, and T. I. Oprea, "Pharos 2023: an integrated resource for the understudied human proteome," *Nucleic Acids Res.* **51** (2023), 10.1093/nar/gkac1033.

[65]B. Wingert, P. Doruker, and I. Bahar, "Activation and speciation mechanisms in class A GPCRs," *J. Mol. Biol.* **434** (2022), 10.1016/j.jmb.2022.167690.

[66]X. Deupi and J. Standfuss, "Structural insights into agonist-induced activation of g-protein-coupled receptors," *Curr. Opin. Struct. Biol.* **21** (2011), 10.1016/j.sbi.2011.06.002.

[67]A. Mitra, A. Sarkar, and A. Borics, "Universal properties and specificities of the β2-adrenergic receptor-g_s protein complex activation mechanism revealed by all-atom molecular dynamics simulations," *Int. J. Mol. Sci.* **22** (2021), 10.3390/ijms221910423.

[68]T. W. Schwartz, T. M. Frimurer, B. Holst, M. M. Rosenkilde, and C. E. Elling, "Molecular mechanism of 7tm receptor activation - a global toggle switch model," *Annu. Rev. Pharmacol. Toxicol.* **46** (2006), 10.1146/annurev.pharmtox.46.120604.141218.

[69]C. E. Elling, T. M. Frimurer, L. O. Gerlach, R. Jorgensen, B. Holst, and T. W. Schwartz, "Metal ion site engineering indicates a global toggle switch model for seven-transmembrane receptor activation," *J. Biol. Chem.* **281** (2006), 10.1074/jbc.M512510200.

[70]L. P. Picard, A. M. Schonegge, and M. Bouvier, "Structural insight into g protein-coupled receptor signaling efficacy and bias between gs and {beta-arrestin", *ACS Pharmacol. Transl. Sci.* **2** (2019), 10.1021/acsptsci.9b00012.

[71]D. Wang, Y. Yao, S. Wang, Y. Hou, L. Zhao, H. Wang, H. Chen, and J. Xu, "Structural insights into m1 muscarinic acetylcholine receptor signaling bias between g$\alpha\beta$ and β-arrestin through BRET assays and molecular docking," *Int. J. Mol. Sci.* **24** (2023), 10.3390/ijms24087356.

[72]E. Lyapina, E. Marin, A. Gusach, P. Orekhov, A. Gerasimov, A. Luginina, D. Vakhrameev, M. Ergasheva, M. Kovaleva, G. Khusainov, P. Khorn, M. Shevtsov, K. Kovalev, S. Bukhdruker, I. Okhrimenko, P. Popov, H. Hu, U. Weierstall, W. Liu, Y. Cho, I. Gushchin, A. Rogachev, G. Bourenkov, S. Park, G. Park, H. J. Hyun, J. Park, V. Gordeliy, V. Borshchevskiy, A. Mishin, and V. Cherezov, "Structural basis for receptor selectivity and inverse agonism in S1P5 receptors," *Nat. Commun.* **13** (2022), 10.1038/s41467-022-32447-1.

[73]L. Yu, L. He, B. Gan, R. Ti, Q. Xiao, H. Hu, L. Zhu, S. Wang, and R. Ren, "Structural insights into sphingosine-1-phosphate receptor activation," *Proc. Natl. Acad. Sci. U. S. A.* **119** (2022), 10.1073/pnas.2117716119.

[74]M. A. Hanson, C. B. Roth, E. Jo, M. T. Griffith, F. L. Scott, G. Reinhart, H. Desale, B. Clemons, S. M. Cahalan, S. C. Schuerer, *et al.*, "Crystal structure of a lipid g protein–coupled receptor," Science **335**, 851–855 (2012).

[75]D. J. Huggins, W. Sherman, and B. Tidor, "Rational approaches to improving selectivity in drug design," *J. Med. Chem.* **55** (2012), 10.1021/jm2010332.

[76]E. A. Wold and J. Zhou, "GPCR allosteric modulators: Mechanistic advantages and therapeutic applications," *Curr. Top. Med. Chem.* **18** (2019), 10.2174/1568026619999190101151837.

[77]P. E. G. F. Ibrahim, F. Zuccotto, U. Zachariae, I. Gilbert, and M. Bodkin, "Accurate prediction of dynamic protein–ligand binding using p-score ranking," *J. Comput. Chem.* **45**, 1762–1778 (2024).